

Conditions for HD Cooling in the First Galaxies Revisited: Interplay between Far-Ultraviolet and Cosmic Ray Feedback in Population III Star Formation

Daisuke Nakauchi¹, Kohei Inayoshi¹, and Kazuyuki Omukai^{1,2}

¹*Department of Physics, Kyoto University, Sakyo, Kyoto 606-8502, Japan*

²*Astronomical Institute, Tohoku University, Aoba, Sendai 980-8578, Japan*

28 March 2018

ABSTRACT

HD dominates the cooling of primordial clouds with enhanced ionization, e.g. shock-heated clouds in structure formation or supernova remnants, relic HII regions of Pop III stars, and clouds with cosmic-ray (CR) irradiation. There, the temperature decreases to several 10 K and the characteristic stellar mass decreases to $\sim 10 M_{\odot}$, in contrast with first stars formed from undisturbed pristine clouds ($\sim 100 M_{\odot}$). However, without CR irradiation, even weak far ultra-violet (FUV) irradiation suppresses HD formation/cooling. Here, we examine conditions for HD cooling in primordial clouds including both FUV and CR feedback. At the beginning of collapse, the shock-compressed gas cools with its density increasing, while the relic HII region gas cools at a constant density. Moreover, shocks tend to occur in denser environments than HII regions. Owing to the higher column density and the more effective shielding, the critical FUV intensity for HD cooling in a shock-compressed gas becomes ~ 10 times higher than in relic HII regions. Consequently, in the shock-compressed gas, the critical FUV intensity exceeds the background level for most of the redshift we consider ($6 \lesssim z \lesssim 15$), while in relic HII regions, HD cooling becomes effective after the CR intensity increases enough at $z \lesssim 10$. Our result suggests that less massive ($\sim 10 M_{\odot}$) Pop III stars may be more common than previously considered and could be the dominant population of Pop III stars.

Key words: stars: formation - stars: Population III - dark ages, reionization, first stars - early Universe.

1 INTRODUCTION

The first generation of stars are believed to have had a significant impact on the cosmic evolution through their radiative, mechanical and chemical feedback (e.g., Ciardi & Ferrara 2005). Stellar extreme-ultraviolet (EUV) photons (> 13.6 eV) ionize the circumstellar gas to form an HII region, thereby initiating the process of the reionization of the intergalactic medium (IGM). Even the single supernova (SN) of a massive ($\gtrsim 150 M_{\odot}$) first-star is able to totally evacuate the gas and suppresses subsequent star formation in the same minihalo (Bromm, Yoshida & Hernquist 2003; Wada & Venkatesan 2003) although some of the materials blown out by the SN of a less-massive ($20\text{--}40 M_{\odot}$) progenitor may fall back again and commence another episode of star formation (Ritter et al. 2012). The ejected gas by a SN contributes to the metal enrichment of the IGM. The extent

of such feedback depends crucially on the initial mass function (IMF), as well as the star formation rate (SFR), of first stars.

Stars formed from the metal-free primordial gas, or Population III (Pop III) stars, have been classified into two sub-populations depending on whether the gas is still in an undisturbed pristine state with a low electron fraction $\sim 10^{-4}$ (Pop III.1), or the gas has already been affected by the radiative or kinematic feedback from pre-existing stars (Pop III.2), following the nomenclature proposed by O’Shea et al. (2008)¹. Despite with the same primordial composition, the thermal evolution of the gas is fairly different in those

¹ Previously, Pop III.2 stars were called in different names from authors to authors, for example, Pop II.5 stars (Mackey, Bromm & Hernquist 2003).

cases, resulting in different characteristic stellar masses. In the standard Λ CDM cosmology, Pop III.1 stars are predicted to be formed in minihalos of $\sim 10^6 M_{\odot}$ (Couchman & Rees 1986; Haiman, Thoul & Loeb 1996; Tegmark et al. 1997). During its protostellar collapse, cooling is entirely by H_2 , which is produced by the following electron-catalyzed reaction (so-called the H^- channel; Peebles & Dicke 1968; Hirasawa, Aizu & Taketani 1969):



With the high value of the minimum temperature 200 K attained at the density $\sim 10^4 \text{ cm}^{-3}$, the fragmentation mass is as large as $\sim 10^3 M_{\odot}$ (Bromm, Coppi & Larson 1999, 2002; Abel, Bryan & Norman 2002; Yoshida et al. 2006), which is set by the Jeans mass at this epoch. In this case, the final mass of formed stars is set by the radiative feedback from the growing protostar, and its value is a few 10 - a few 100 M_{\odot} , much higher than the present-day counterpart (Omukai & Palla 2001, 2003; McKee & Tan 2008; Yoshida, Omukai & Hernquist 2008; Hosokawa et al. 2011; Stacy, Greif & Bromm 2012; Susa 2013; Hirano et al. 2014). On the other hand, Pop III.2 stars are formed from the metal-free gas affected either by the radiative or kinematic feedback from earlier generation of stars, typically in atomic-cooling halos with virial temperatures $\gtrsim 10^4$ K (O’Shea & Norman 2008; Greif et al. 2008). An example of Pop III.2 stars is those formed in the relic HII regions of defunct Pop III stars (Kitayama et al. 2004; Whalen, Abel & Norman 2004; Yoshida et al. 2007a; Abel, Wise & Bryan 2007). In this case, a larger amount of H_2 is produced ($\sim 10^{-3}$) via the H^- channel (Eqs. 1 and 2) than in the Pop III.1 case ($\sim 10^{-4}$) (e.g., O’Shea et al. 2005). Once the temperature plummets below 150 K by this H_2 cooling, deuterium is rapidly converted into HD via the exothermic reaction,



This cooling by HD lowers the temperature further to ~ 30 K (e.g., Nagakura & Omukai 2005). The characteristic mass of stars formed in such an environment is predicted to be $\sim 10 M_{\odot}$ (Uehara & Inutsuka 2000; Nakamura & Umemura 2002; Mackey, Bromm & Hernquist 2003; Machida et al. 2005; Nagakura & Omukai 2005; Johnson & Bromm 2006; Yoshida et al. 2007a; Yoshida, Omukai & Hernquist 2007; Wolcott-Green & Haiman 2011; Hosokawa et al. 2012). That is, Pop III.2 stars may be typically less massive than preceding Pop III.1 stars although they are more massive than ordinary present-day stars².

² It should be noted that recent numerical simulations suggest that there is another possible pathway of lower-mass primordial star formation in Pop III.1 case, like disk fragmentation (e.g., Greif et al. 2012). So the typical mass-scale of Pop III.1 stars remains an open question.

With high effective temperatures ($\sim 10^5$ K) (Schaerer 2002), massive Pop III stars emit a copious amount of far-UV (FUV) photons in the Lyman-Werner (LW) bands (11.2-13.6 eV). The FUV radiation field photodissociates H_2 , thereby prohibiting efficient cooling in the primordial gas. Even a single massive Pop III star emits enough FUV photons to suppress the subsequent star formation in the same halo (Omukai & Nishi 1999; Glover & Brand 2001). In addition, the gas in a minihalo is fairly vulnerable to the external irradiation of FUV photons and thus the number of Pop III.1 stars formed can be severely regulated by the FUV background (e.g., Haiman, Rees & Loeb 1997). On the other hand, Pop III.2 star formation in more massive halos still goes on by atomic cooling even under the FUV background and is not strongly affected. (Haiman et al. 1997; O’Shea & Norman 2008). This indicates the possibility that Pop III.2 stars can be the major population of primordial stars and significant sources of radiative and chemical feedback to subsequent star formation (Trenti & Stiavelli 2009; de Souza, Yoshida & Ioka 2011). Moreover, the Pop III.2 star-formation epoch may have lasted until redshifts as low as $z \sim 6$ (Tornatore, Ferrara & Schneider 2007; de Souza, Yoshida & Ioka 2011; Johnson, Dalla Vecchia & Khochfar 2013). If so, gamma-ray bursts (GRBs) or SNe of Pop III.2 stars are detectable with future facilities, which allow us to peer into the nature of primordial stars (Nakauchi et al. 2012; Whalen et al. 2013; Tanaka, Moriya & Yoshida 2013).

Later, however, it was found that HD formation is strongly suppressed in the presence of even a weak FUV radiation field (Yoshida et al. 2007b; Wolcott-Green & Haiman 2011) since the slight photodissociation of H_2 causes the significant reduction of the HD fraction. Without HD cooling, the thermal evolution of a Pop III.2 star-forming gas becomes identical to the Pop III.1 case, resulting in Pop III.2 stars having similar masses to Pop III.1 stars. However, this is not yet the conclusive result since the previous studies have not properly taken account of the following effects, which favors HD formation/cooling.

In the galaxy formation epoch, shocks occur ubiquitously, for example, associating with the virialization of halos or SN explosions. In a shocked gas, the enhanced ionization degree enables efficient H_2 /HD formation and cooling (Uehara & Inutsuka 2000; Mackey, Bromm & Hernquist 2003; Johnson & Bromm 2006; Greif et al. 2008). For a strong shock, the post-shock gas is compressed isobarically with its cooling, i.e., the temperature decreases with increasing the density (e.g., Shapiro & Kang 1987). On the other hand, for the free-falling cloud in a relic HII region, rapid cooling makes the temperature to plummet almost isochorically, i.e., the temperature decreases at a constant density (Yoshida et al. 2007b; Johnson & Bromm 2006; Wolcott-Green & Haiman 2011). With the higher column density, the FUV radiation field is more effectively shielded for the post-shock flow than in the relic HII region, resulting in the lower FUV flux in the former case. Nonetheless, in the previous studies (e.g., Wolcott-Green & Haiman 2011), the post-shock flows are treated without the proper account of the isobaric nature of evolution.

Associated with star-formation activities, not only the FUV background, but also the cosmic ray (CR) background is expected to be generated by way of the CR acceleration in SN remnants. CR irradiation promotes H₂ and HD formation/cooling by enhancing the ionization degree (Jasche, Ciardi, & Enßlin 2007; Stacy & Bromm 2007; Inayoshi & Omukai 2011). Thus, CR irradiation is able to counteract with the negative feedback of FUV radiation. However, only either FUV or CR irradiation has been considered in the previous studies (Jasche, Ciardi, & Enßlin 2007; Stacy & Bromm 2007; Wolcott-Green & Haiman 2011) and their combined effects have not been fully understood.

In this paper, we study the conditions for HD cooling to become important in Pop III.2 star formation under the presence of both FUV and CR backgrounds. We calculate the temperature and chemical evolution of (i) a cloud compressed by plane-parallel steady shocks (Shapiro & Kang 1987), and of (ii) a free-falling cloud in a relic HII region. We find that the critical value for FUV intensity above which HD cooling is quenched is about an order of magnitude higher in the former than in the latter case. Also the critical FUV intensity increases with increasing CR intensity. We also estimate the background FUV and CR intensities from theoretically predicted values for the SFR in the high-redshift universe. By comparing the background FUV intensity with the critical value, we conclude that the HD mode of Pop III.2 star formation is fairly common at the galaxy formation epoch.

The rest of this paper is organized as follows. In §2, we describe the numerical model and initial conditions for our calculation. In §3, we present the results for the free-falling clouds in relic HII regions and for the clouds compressed either by the virialization shock or by the SN blast wave. We also present the critical FUV intensity for HD cooling as a function of the CR intensity. In §4, we estimate the background FUV and CR intensities in high-redshift universe, and discuss whether the HD cooling condition is satisfied at these epochs. After discussing the implications and uncertainties of our study in §5, we summarize our findings in §6.

2 MODEL

In this section, we present our model for calculating the thermal and chemical evolution of primordial clouds.

2.1 Formulation

Here, we first describe the method of calculation for the free-falling cloud in a relic HII region and then for the shock-compressed gas in structure formation or an SN explosion. We use the one-zone model, where we focus on the evolution of the central core for the free-falling cloud and of the coolest gas layer for the shock-compressed gas before the self-gravity becomes effective by using the plane-parallel and steady shock approximation.

2.1.1 Free-falling Cloud in a relic HII region

When a Pop III star dies and collapses directly to a black hole (BH), the gas in the relic HII region surrounding the star begins to recombine and cool to form a subsequent star (Kitayama et al. 2004; Whalen, Abel & Norman 2004; Yoshida et al. 2007a; Yoshida, Omukai & Hernquist 2007; Abel, Wise & Bryan 2007). Here, we assume that the formed BH has no influence on the evolution of the gas in the relic HII region for simplicity. At first, the baryon mass in the relic HII region is too small for the gas to contract by self-gravity, but the gas loses pressure-support by efficient radiative cooling and contracts being attracted by the gravitational potential of the DM halo. After the temperature decreases so that the Jeans mass becomes lower than the HII region mass, the gas begins to contract in the almost free-fall way by self-gravity. Owing to its high pressure, the gas in the HII region is accelerated monotonically with radius up to a supersonic velocity and expands into the interstellar medium (Whalen et al. 2004; Kitayama et al. 2004). However, our model does not take into account the initial velocity profile within the HII region for simplicity. The following prescription is the same as the previous studies (Johnson & Bromm 2006; Yoshida, Omukai & Hernquist 2007; Wolcott-Green & Haiman 2011).

An isolated cloud collapsing at the rate close to free-fall by its self-gravity develops a core-envelope structure (Larson 1969; Penston 1969), consisting of a nearly Jeans-scale core with the constant density and an envelope where the density decreases radially as $\rho \propto r^{-2}$. In our one-zone model, we follow the evolution of the physical quantities at the core center (Omukai 2001). Since collapse proceeds roughly at the free-fall rate, the density evolves as

$$\frac{d\rho}{dt} = \frac{\rho}{t_{\text{ff}}}, \quad (4)$$

where $t_{\text{ff}} = \sqrt{3\pi/32G\rho}$ is the free-fall time and G the gravitational constant. Temperature evolution follows the energy equation:

$$\frac{de}{dt} = -P \frac{d}{dt} \left(\frac{1}{\rho} \right) - \frac{\Lambda_{\text{net}}}{\rho}, \quad (5)$$

where e is the internal energy per unit mass, P the pressure, Λ_{net} the net cooling rate per unit volume. To supplement the equations above, the ideal-gas equation of state $P = \rho k_{\text{B}} T / \mu m_{\text{H}}$ is used, where k_{B} is the Boltzmann constant, m_{H} the proton mass and μ the mean molecular weight. Using the ratio of specific heat γ , specific energy is related to pressure as $e = P/\rho(\gamma - 1)$. Throughout this paper, we take $\mu = 1.2$ and $\gamma = 5/3$ neglecting molecular contribution. Considering that the size of the contracting core is half the Jeans length $\lambda_{\text{J}} = \sqrt{\pi k_{\text{B}} T / G \rho \mu m_{\text{H}}}$, we calculate the column density of the core as $N_{\text{J}} = n_{\text{H}} \lambda_{\text{J}} / 2$ (Inayoshi & Omukai 2011). In this case, the initial size of this region is estimated as ~ 1 kpc, which is an overestimation compared to the typical size of an HII region $R_{\text{HII}} \sim 100$ pc (Whalen et al. 2004; Kitayama et al. 2004). However, at the beginning of collapse, owing to the low gas density and H₂ fraction, the H₂ column density will be too low for effectively shielding the gas from the

FUV field, and the above overestimation will not matter for estimating the shielding factor.

In our model of free-fall collapse, the collapse equation and the energy equation (Eqs. 4, 5) are decoupled and feedback from thermal pressure is not included for simplicity. In the runaway-collapse phase, an isothermal cloud collapses approximately at a free-fall rate (Larson 1969; Penston 1969). Although the pressure gradient is not negligible, the deviation of the collapse time from free fall is only by a factor of 1.58 (Larson 1969). For a non-isothermal case, the deviation is represented as a monotonically increasing function of the effective adiabatic index γ of the cloud in equations 7-9 of Omukai et al. (2005). For example, the collapse time becomes ~ 3 times longer than the free-fall time for $\gamma = 1.2$. If we use this generalized collapse time for the collapse equation, the collapse equation 4 is coupled with the energy equation 5. However, we find that the effective adiabatic index becomes smaller than 1.2 for most of the evolutionary trajectory, and the deviation from free-fall may be at most by a factor of a few. Thus, feedback from thermal pressure may change our results little.

Here, we consider that an overdense region collapsing within an HII region is large enough. Then, since the overdense region is strongly bounded by the gravitational field of DM and gas, it contracts by the gravitational force which exceeds the pressure force from its less-dense surroundings. Therefore, the compression of the overdense region by external pressure may be neglected, and it will collapse roughly at a free-fall rate.

Although our formulation does not include DM gravity, it becomes significant at the beginning of gas evolution. Then, we recalculate the evolution of the gas in relic HII regions taking account of DM gravity by modifying ρ in t_{ff} of Eq. (4) to $\rho + \rho_{\text{DM}}$, but we find little change in our results. Here, $\rho_{\text{DM}} = 1.3 \times 10^{-24} \text{ g cm}^{-3}$ is the mean DM mass density of a virialized halo at $z = 15$.

2.1.2 Shock-Compressed Gas

After the passage of a blast wave, which is generated in structure formation or an SN explosion, the post-shock gas has a very high temperature due to shock heating and it cools and contracts with the radiative cooling time. At first, self-gravity is not effective in the shocked gas layer. We focus on the evolution of the most cooled gas layer, assuming that the post-shock gas layer is plane-parallel and the flow is steady (Shapiro & Kang 1987; Yamada & Nishi 1998; Inayoshi & Omukai 2012). The initial condition of a shock-compressed gas is characterized by two parameters: the pre-shock density ρ_0 and the velocity of the shock front v_0 . In the strong shock limit, the physical quantities just behind the shock front are given by the Rankine-Hugoniot relation:

$$\rho_1 = 4\rho_0, \quad (6)$$

$$v_1 = \frac{1}{4}v_0, \quad (7)$$

$$T_1 = \frac{3}{16} \frac{\mu m_{\text{H}}}{k_{\text{B}}} v_0^2 \quad (8)$$

$$\sim 1.1 \times 10^4 \left(\frac{\mu}{1.2}\right) \left(\frac{v_0}{20 \text{ km/s}}\right)^2 \text{ K},$$

where the subscripts 0 and 1 refer to the pre- and post-shock quantities, respectively. Behind the shock front, the flow evolution is described by

$$\rho_1 v_1 = \rho v, \quad (9)$$

$$\rho_1 v_1^2 + P_1 = \rho v^2 + P, \quad (10)$$

along with the energy equation (5). The column density of the post-shock gas can be estimated from

$$N_{\text{H}}(t) = n_{\text{H},0} v_0 t, \quad (11)$$

where $n_{\text{H},0}$ is the number density in the pre-shock gas and t is the time since the shock occurs.

Rapid cooling in the post-shock layer leads to the formation of a dense gas shell, which eventually becomes gravitationally unstable and fragments. For the SN shock, we assume that fragmentation occurs when the column density of the post-shock layer N_{H} exceeds that in the Jeans length N_{J} (Safranek-Shrader, Bromm & Milosavljević 2010; Inayoshi & Omukai 2012):

$$N_{\text{H}}(t) = N_{\text{J}}. \quad (12)$$

For the structure-formation shock, the mass of the post-shock layer is doubled compared to the SN case, since in one dimension, two flows collide to form the shocked region and two shock fronts propagate in opposite directions to each other. In this case, fragmentation occurs under the condition:

$$2N_{\text{H}}(t) = N_{\text{J}}. \quad (13)$$

In addition to them, for fragmentation, the growth time of a perturbation, which is approximately given by the local free-fall time t_{ff} , must be shorter than the contraction time of the layer, i.e., the cooling time t_{cool} (Yamada & Nishi 1998). We have confirmed this condition is always satisfied at the fragmentation epoch determined by the column-density conditions given above. After fragmentation, each fragment or clump begins to contract by its self-gravity. We also follow its evolution by the same one-zone model as in Sec. 2.1.1.

2.2 Thermal and Chemical Processes

The net cooling rate Λ_{net} in Eq. (5) consists of the following terms:

$$\Lambda_{\text{net}} = \Lambda_{\text{H}} + \Lambda_{\text{H}_2} + \Lambda_{\text{HD}} - \Gamma_{\text{CR}}, \quad (14)$$

where Λ_{H} , Λ_{H_2} and Λ_{HD} are the radiative cooling rates by H Lyman- α line emission, H₂-line emission and HD-line emission, respectively, and Γ_{CR} is the CR heating rate. We adopt the cooling rates Λ_{H} from Glover & Jappsen (2007),

Λ_{H_2} from Galli & Palla (1998), and Λ_{HD} from Galli & Palla (2002). Since each CR ionization associates with heating of ~ 6 eV (Spitzer & Scott 1969),

$$\Gamma_{\text{CR}} \sim 9.6 \times 10^{-12} n(\text{H}) \zeta_{\text{CR}} \text{ erg cm}^{-3} \text{ s}^{-1}, \quad (15)$$

where ζ_{CR} is the hydrogen ionization rate by CRs, and $n(\text{H})$ is the number density of hydrogen atoms. At densities we consider ($\lesssim 10^7 \text{ cm}^{-3}$), the contribution from chemical cooling and heating is small and is neglected in this paper (Omukai 2001).

Our chemical network includes following 11 species: H, H₂, e, H⁺, H₂⁺, H⁻, D, HD, D⁺, HD⁺ and D⁻. The deuterium fraction is set to 4.0×10^{-5} , and the He chemistry is neglected since it is thermally inert in the temperature range we consider. Chemical reactions include 18 hydrogen collisional reactions in Table 1 of Yoshida et al. (2006), 18 deuterium collisional reactions in Table 1 of Nakamura & Umemura (2002), photo-dissociation of H₂, HD, and H⁻, and CR ionization. For collisional reactions, we use the updated rate coefficients by Glover & Abel (2008). The photo-dissociation rate coefficients are taken from Omukai (2001) and Wolcott-Green & Haiman (2011), and the H₂ and HD shielding factors are from Wolcott-Green & Haiman (2011). For the shielding factors, we take account of the Doppler shift due to the bulk motion of the cloud as in Omukai (2001) for the free-falling case and in Omukai (2007) for the shock-compressed case. The stellar radiation field is assumed to have the diluted black-body spectrum with the temperature of 10^4 K, resembling that from a Pop II star cluster, and its intensity is parameterized by $J_{21} \equiv J_{\nu_{\text{Ly}}}/10^{-21} \text{ erg cm}^{-2} \text{ s}^{-1} \text{ Hz}^{-1}$, where $J_{\nu_{\text{Ly}}}$ is the intensity at the Lyman limit. The CR ionization rate of neutral hydrogen ζ_{CR} is treated as a free parameter, since the CR intensity at the high-redshift universe is highly uncertain. However, the CR intensity may be related with the star-forming activity, and the SFR at $z \sim 10$ is theoretically estimated to be no more than the present-day value (e.g., Tornatore et al. 2007; Trenti & Stiavelli 2009; Johnson et al. 2013). We thus consider the CR intensity in the range of $\zeta_{\text{CR}} \lesssim 10^{-17} \text{ s}^{-1}$, which are smaller than the Galactic value $10^{-17} \text{ s}^{-1} \lesssim \zeta_{\text{CR}} \lesssim 10^{-15} \text{ s}^{-1}$ (Hayakawa, Nishimura & Takayanagi 1961; Spitzer & Tomasko 1968; Webber 1998; McCall et al. 2003; Indriolo et al. 2007).

2.3 Initial Conditions

2.3.1 Relic HII Region

In the relic HII region of a defunct Pop III star, a primordial cloud begins to collapse from a highly ionized state. The temperature and density in the relic HII region are almost uniform with $1\text{-}3 \times 10^4$ K and $0.1\text{-}1 \text{ cm}^{-3}$ (Kitayama et al. 2004; Whalen et al. 2004; Abel, Wise & Bryan 2007; Yoshida et al. 2007a). We thus adopt $T_0 = 3 \times 10^4$ K and $n_{\text{H},0} = 0.3 \text{ cm}^{-3}$ as the fiducial initial values, and also study the cases with higher and lower densities $n_{\text{H},0} = 0.03, 3 \text{ cm}^{-3}$ to see the dependence on the initial density. We set the initial chemical abundances as $y_0(\text{H}^+) = 1.0$, $y_0(\text{D}^+) = 4.0 \times 10^{-5}$,

Table 1. Initial chemical composition in the shock-compressed gas

v_0 (km s ⁻¹)	$y_0(\text{H})$	$y_0(\text{H}^+)$	$y_0(\text{D})$	$y_0(\text{D}^+)$
20	0.99	0.01	3.96×10^{-5}	4.0×10^{-7}
100	0.3	0.7	1.2×10^{-5}	2.8×10^{-5}

$y_0(e) = y_0(\text{H}^+) + y_0(\text{D}^+)$, and $y(i) = 0$ for other species, where $y(i)$ is the fractional abundance of the i -th species to the hydrogen nuclei.

2.3.2 Shock-Compressed Gas

We consider two kinds of shocks which occur in the virialization of halos and SN explosions. Here, we need to specify the shock velocity v_0 , pre-shock density $n_{\text{H},0}$, and initial chemical abundance $y_0(i)$ for each case.

For the virialization shock, the mean gas number density within the virialized halo is estimated as (Clarke & Bromm 2003)

$$n_{\text{H},0} \sim 0.13 \left(\frac{1+z}{15} \right)^3 \text{ cm}^{-3}. \quad (16)$$

However, according to the recent studies on first galaxy formation, the shock front does not sustain at the virial radius and its location shrinks inward owing to efficient Ly- α emission (Wise & Abel 2007; Wise, Turk & Abel 2008). Proto-galaxies accrete gas via cold flows in dense filaments, with the infall velocity of $\sim 20 \text{ km s}^{-1}$. Such cold flows penetrate deep inside the halo and collide each other to form virialization shocks with pre-shock densities $1\text{-}10^3 \text{ cm}^{-3}$, much higher than in Eq. (16). Considering this effect, we adopt $(v_0, n_{\text{H},0}) = (20, 1.0)$ as the fiducial values for the pre-shock gas.

The shocked gas behind a SN blast wave cools and is compressed significantly after the SN remnant enters the pressure-driven expansion phase (Machida et al. 2005; Nagakura, Hosokawa & Omukai 2009; Chiaki, Yoshida & Kitayama 2013). The shock velocity early in this phase is $\sim 100 \text{ km s}^{-1}$ (Machida et al. 2005; Nagakura et al. 2009; Chiaki et al. 2013). The pre-shock density is comparable to the density in relic HII regions $0.1\text{-}1 \text{ cm}^{-3}$, since core-collapse SNe explode within HII regions which their progenitors produce. Hence, we adopt $(v_0, n_{\text{H},0}) = (100, 0.1)$ as the fiducial values for the SN shock.

Shapiro & Kang (1987) and Kang & Shapiro (1992) studied the chemical composition in the primordial gas just behind a shock front. We adopt their results as the initial composition in the shock-compressed gas, which are summarized in Table 1 for the virialization and SN shocks. The fractions of species not presented in Table 1 are set to zero, except for the electron fraction $y_0(e) = y_0(\text{H}^+) + y_0(\text{D}^+)$.

3 RESULTS

3.1 Relic HII region

Here, we present the results for the free-falling cloud in a relic HII region. We also find the critical FUV intensity above which HD cooling is suppressed for the different values of the CR intensity.

3.1.1 Thermal Evolution

First, we see the results without CR irradiation to extract the FUV effect alone. Fig. 1 shows the temperature evolution, and Fig. 2 shows the fractions of (a) H₂, (b) electron, and (c) HD, for five different FUV intensities: $J_{21} = 0, 0.01, 0.1, 1,$ and 10 , both as a function of the number density n_{H} . The temperature first drops isochorically to ~ 8000 K via efficient Ly- α cooling in all the cases in Fig. 1, and the subsequent behavior depends on the FUV intensities. The same results are obtained in Johnson & Bromm (2006), Yoshida, Omukai & Hernquist (2007), and Wolcott-Green & Haiman (2011).

In the absence of FUV irradiation ($J_{21} = 0$), abundant H₂ with the fraction $\sim 10^{-3}$ forms via the H⁻ channel (Eqs. 1 and 2) owing to the high initial ionization degree (solid line in Fig. 2a). The cooling by this enhanced H₂ makes the temperature to fall below $\simeq 200$ K, the minimum value attainable in the primordial pristine gas, where the ionization degree is only $\sim 10^{-4}$ (Omukai 2001). Once the temperature reaches $\lesssim 150$ K, the exothermic reaction (Eq. 3) converts most of the deuterium into HD (solid line in Fig. 2c). HD cooling further drops the temperature to the minimum value ~ 30 K at density $\sim 10^5$ cm⁻³, which is the critical density for HD to reach local thermodynamic equilibrium. Toward higher density, the temperature increases gradually by compressional heating. At the temperature minimum, the parent cloud is considered to fragment into clumps with the Jeans mass of $\lesssim 100 M_{\odot}$ (Yoshida et al. 2007b; McGreer & Bryan 2008). We call hereafter this mode of star formation as *HD-Pop III star formation*, in contrast to *H₂-Pop III star formation*, where H₂ is the sole coolant during proto-stellar collapse.

With FUV irradiation, the temperature becomes higher owing to the photodissociation of the coolants, H₂ and HD (Fig. 2a, c). With J_{21} as low as 0.01, the evolutionary track is similar to that of $J_{21} = 0$, although with slightly higher temperature. With intensity $J_{21} = 0.1$, the H₂ fraction is reduced to $\sim 10^{-4}$, and the temperature does not reach the regime of efficient HD formation/cooling (short-dashed line in Fig. 2a, c). With the even higher FUV intensity $J_{21} \geq 1.0$, photodissociation strongly reduces the H₂ fraction at low densities (dotted and dot-dashed lines in Fig. 2a). The clouds contract isothermally at ~ 8000 K by Ly- α cooling until $n_{\text{H}} \sim 10$ cm⁻³ for $J_{21} = 1.0$ (~ 100 cm⁻³ for $J_{21} = 10$, respectively), where the H₂ self-shielding against FUV radiation becomes effective. Thereafter, the temperature drops first almost vertically to ~ 2000 K and then gradually to ~ 300 K by H₂ cooling. In the cases with $J_{21} \geq 0.1$, without HD cooling, the gas cools only to the minimum temperature ~ 200 K by H₂ cooling at $\sim 10^3$ - 10^4 cm⁻³ as in

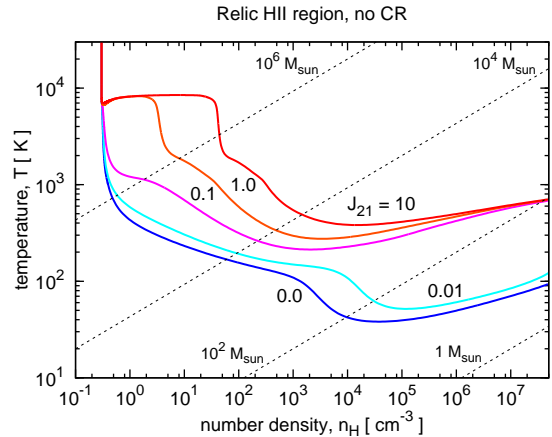


Figure 1. FUV effect on thermal evolution of clouds in relic HII region. No CR irradiation is considered. The initial density is $n_{\text{H},0} = 0.3$ cm⁻³. Different lines correspond to the different FUV intensities: $J_{21} = 0.0, 0.01, 0.1, 1.0,$ and 10 from bottom to top. The thin dashed lines indicate the constant Jeans masses.

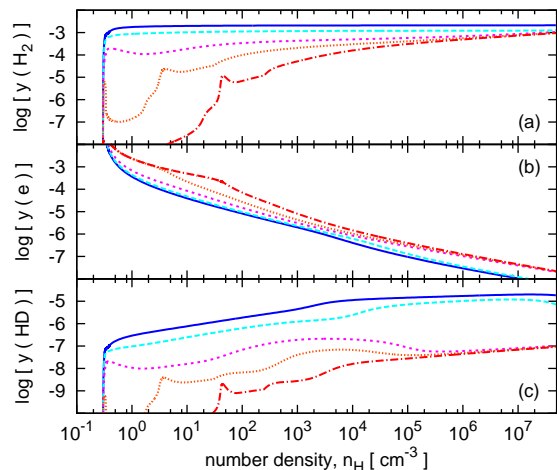


Figure 2. Chemical fractions of (a) H₂, (b) e, and (c) HD in the same clouds as in Fig. 1. In each panel, different lines correspond to the different FUV intensities: $J_{21} = 0.0$ (solid), 0.01 (long-dashed), 0.1 (short-dashed), 1.0 (dotted), and 10 (dot-dashed).

the case of Pop III.1 star formation. Namely, star formation proceeds in the H₂-Pop III mode. In this mode, the clouds fragment into rather massive clumps of $\sim 10^3 M_{\odot}$. Note that, in the high density regime ($\gtrsim 10^5$ cm⁻³), all the evolutionary tracks converge to either of the two tracks, one by HD cooling for $J_{21} \leq 0.01$ or the other by H₂ cooling for $J_{21} \geq 0.1$.

Next, we see the results with CR irradiation on cloud evolution, as shown in Figs. 3 and 4, for the cases with FUV intensity $J_{21} = 0.1$. The different lines in the Figures show

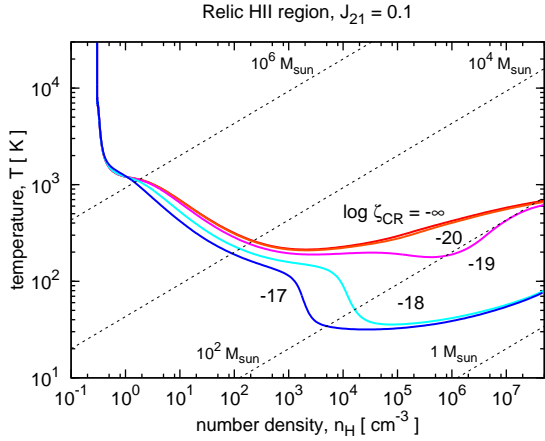


Figure 3. CR effect on thermal evolution of clouds in relic HII regions. The FUV intensity is fixed to $J_{21} = 0.1$, and the initial density to $n_{H,0} = 0.3 \text{ cm}^{-3}$. Different lines correspond to the different CR intensities: $\log \zeta_{\text{CR}} (\text{s}^{-1}) = -\infty, -20, -19, -18$, and -17 . The thin dashed lines indicate the constant Jeans masses.

different values of the CR intensity: $\log \zeta_{\text{CR}} (\text{s}^{-1}) = -\infty$ (i.e., $\zeta_{\text{CR}} = 0$), $-20, -19, -18$ and -17 . Recall that, with $J_{21} = 0.1$, HD cooling is suppressed without CR irradiation. As seen in Fig. 3, with higher ζ_{CR} , the temperature becomes lower. This is because the elevated ionization degree by CR ionization causes more efficient H_2 formation and cooling (see Fig. 4), which outweighs the effect of CR ionization heating. For $\log \zeta_{\text{CR}} \geq -18$, the temperature falls below 150 K, where the HD fraction increases significantly, owing to the enhanced H_2 cooling (solid and long-dashed lines in Fig. 4c). By HD cooling, the temperature further drops to ~ 30 K, and HD-Pop III star formation is realized in these cases. In this way, CR ionization can compensate the negative feedback of FUV photodissociation.

Since in our model for the free-falling cloud, the collapse equation (eq. 4) is decoupled from the energy equation (eq. 5), the collapse time becomes the same for the same initial density and is obtained as $t_{\text{collapse}} \sim 200$ Myr for $n_{H,0} = 0.3 \text{ cm}^{-3}$. The Hubble time is estimated as $t_H(z) = 500 \left((1+z)/10 \right)^{-3/2}$ Myr and this is roughly equal to the galaxy merger time. We find that the collapse timescale estimated above is smaller than the Hubble time for $z < 15$. Moreover, in the early universe we consider, the halo does not have an angular momentum large enough to form a rotation-supported disk which is comparable to the protogalaxy scale (Abel et al. 2002). Thus, the gas cloud in a relic HII region may remain isolated without being affected by the protogalaxy rotation and merger, and star formation there proceeds within the local Hubble time.

3.1.2 Critical FUV intensity for HD Cooling

We have learned that with the FUV intensity exceeding a critical value $J_{21,\text{crit}}$, HD cooling is totally suppressed even in initially ionized clouds. In addition, the value of the crit-

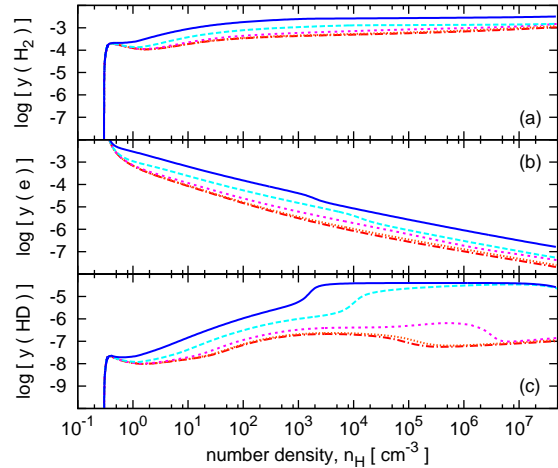


Figure 4. (a) H_2 , (b) e , and (c) HD fractions for the same clouds as in Fig. 3. In each panel, the different lines correspond to the different values of CR intensity: $\log \zeta_{\text{CR}} (\text{s}^{-1}) = -\infty$ (dot-dashed), -20 (dotted), -19 (short-dashed), -18 (long-dashed), and -17 (solid).

ical FUV intensity is elevated under CR irradiation. In Fig. 5, the critical FUV intensity $J_{21,\text{crit}}$ is plotted as a function of ζ_{CR} for initial densities $n_{H,0} = 0.03$ (dashed), 0.3 (solid) and 3 (dot-dashed) cm^{-3} . In finding the value of $J_{21,\text{crit}}$, we judge HD cooling is effective if the following two conditions are satisfied: (i) the minimum temperature at $> 10^5 \text{ cm}^{-3}$ is less than 100 K, and (ii) the HD-cooling rate exceeds a half of the total (i.e. the sum of compressional and CR) heating rate at some moment. These two conditions are imposed to discriminate whether the high-density temperature tracks are either those by H_2 cooling or by HD cooling. In the fiducial case of $n_{H,0} = 0.3 \text{ cm}^{-3}$ (solid line), the critical intensity is $J_{21,\text{crit}} = 0.03$ for the negligible CR intensity ($\zeta_{\text{CR}} \sim 10^{-20} \text{ s}^{-1}$), in accord with previous studies (Yoshida et al. 2007b; Wolcott-Green & Haiman 2011). The critical intensity $J_{21,\text{crit}}$ increases with the CR strength ζ_{CR} , since strong enough CR irradiation enables efficient HD cooling even under an intense FUV field.

In the weak CR regime $\zeta_{\text{CR}} \lesssim 3 \times 10^{-19} \text{ s}^{-1}$, the electrons present initially, rather than those produced by CR ionization, work as catalysts for the H_2 formation reaction. Abundant H_2 is formed if the self-shielding against the FUV field becomes effective before the ionization degree is reduced significantly by recombination. Since the self-shielding is more effective for larger column densities and thus for larger $n_{H,0}$, more H_2 is formed under the same FUV intensity. This results in higher $J_{21,\text{crit}}$ for higher $n_{H,0}$. On the other hand, in the strong CR regime ($\zeta_{\text{CR}} \gtrsim 3 \times 10^{-19} \text{ s}^{-1}$), CR ionization provides the necessary electrons for abundant H_2 formation. Moreover, with a FUV field as high as $J_{21,\text{crit}}$, the shielding against the FUV field becomes effective and H_2 formation occurs only after the density is significantly increased from the initial value. Therefore, the evolutionary

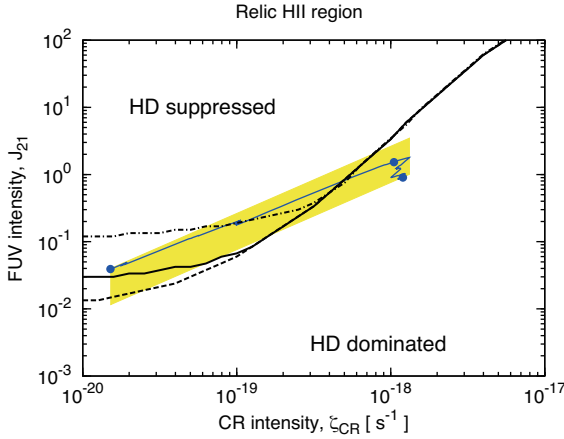


Figure 5. The critical FUV intensity $J_{21,\text{crit}}$ for HD cooling as a function of the CR intensity ζ_{CR} . Each curve corresponds to the different initial densities: $n_{\text{H},0} = 0.03$ (dashed), 0.3 (solid) and 3 (dot-dashed) cm^{-3} . Below $J_{21,\text{crit}}$, HD dominates the cooling in the course of cloud collapse. The shaded region shows the background FUV and CR intensities estimated from Eqs. (18) and (21) with $6 \lesssim z \lesssim 15$ and $10^{-4} \lesssim \Psi_{*,\text{II}}(z)/M_{\odot}\text{yr}^{-1}\text{Mpc}^{-3} \lesssim 3 \times 10^{-2}$. The blue thin-solid line shows the evolution of the background intensities evaluated using the Pop II SFR $\Psi_{*,\text{II}}(z)$ of Johnson et al. (2013). The blue points refer to values at $z = 15, 10$ and 6 from left to right.

track and critical FUV intensity $J_{21,\text{crit}}$ do not depend on the initial density.

3.2 Shock-compressed Gas

Here, we present the results for a shock-compressed gas in the two cases of the shock velocity: (i) $v_0 = 20 \text{ km s}^{-1}$ (virialization shock) and (ii) 100 km s^{-1} (SN shock), respectively.

3.2.1 Virialization Shock

First, to see the FUV effect on the gas compressed by the virialization shock ($v_0 = 20 \text{ km s}^{-1}$), the results are shown for the cases without CR irradiation in Figs. 6 and 7. Just behind the shock front, the gas is heated to $\gtrsim 10^4 \text{ K}$ and then cools immediately to $\sim 8000 \text{ K}$ by Ly- α cooling. With the negligible or weak FUV field ($J_{21} \lesssim 0.01$), H_2 forms abundantly owing to the high ionization degree (~ 0.01) in the post-shock gas (solid and long-dashed lines in Fig. 7a, b). As in the relic HII region, the gas enters the HD formation regime ($\lesssim 150 \text{ K}$) by H_2 cooling (solid and long-dashed lines in Fig. 7c), and the temperature further decreases to $\sim 30 \text{ K}$ by HD cooling. As long as the cooling time is shorter than the free-fall time, the post-shock gas is compressed almost isobarically (e.g., Shapiro & Kang 1987; Yamada & Nishi 1998). However, below $\sim 30 \text{ K}$, HD cooling is not efficient anymore, and the cooling time exceeds the free-fall time. When the sufficient mass for gravitational instability accumulates in the dense layer, it fragments into clumps of approximately the Jeans mass $\sim 100 M_{\odot}$, which then continue

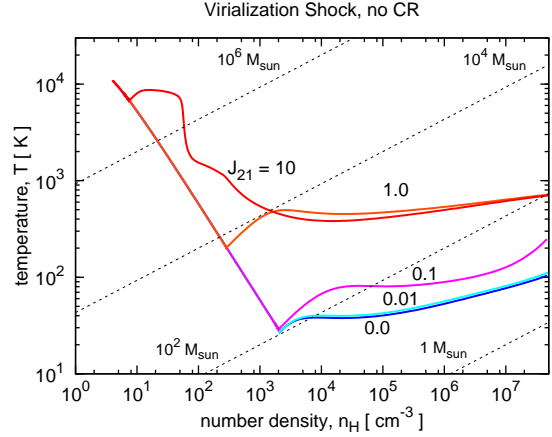


Figure 6. FUV effect on thermal evolution of shock-compressed clouds by virialization. No CR irradiation is considered. The initial density and shock velocity are taken as fiducial values: $n_{\text{H},0} = 1.0 \text{ cm}^{-3}$ and $v_0 = 20 \text{ km s}^{-1}$. Different lines correspond to the different FUV intensities: $J_{21} = 0.0, 0.01, 0.1, 1.0$, and 10 .

collapsing by HD cooling in the free-fall manner. This late-time temperature evolution is along the HD-cooling track, like the free-falling clouds in relic HII regions ($J_{21} = 0.0$ in Fig. 1). For $J_{21} = 0.1$, the isobaric contraction proceeds in the same way until $\sim 30 \text{ K}$ as with the weaker FUV case. However, during the dense gas layer stays at $\sim 30 \text{ K}$ until the Jeans instability sets in, the HD fraction is significantly reduced by electron recombination and H_2/HD photodissociation (short-dashed lines in Fig. 7c). As a result, HD cooling does not become important in the subsequent free-fall phase and temperature evolution eventually converges to the H_2 -cooling track. For $J_{21} \geq 1.0$, strong FUV radiation completely quenches HD cooling and massive clumps of $\sim 10^4 M_{\odot}$ will be formed. Especially, in the case of $J_{21} = 10$, fragmentation takes place early at $\sim 8000 \text{ K}$. The subsequent free-fall evolution is similar to that of the free-falling clouds in relic HII regions with $J_{21} \geq 1.0$ (Fig. 1).

Next, we see the CR effect for the case with FUV intensity $J_{21} = 1.0$. The results are shown in Figs. 8 and 9. Recall that, with $J_{21} = 1.0$, HD cooling is suppressed in the absence of CR irradiation. As in the case of the relic HII region, more H_2 is formed by CR ionization (Fig. 9a, b) and the temperature becomes lower by the enhanced H_2 cooling. With the CR strength exceeding $\zeta_{\text{CR}} = 10^{-18} \text{ s}^{-1}$, most deuterium is converted into HD (long-dashed and solid lines in Fig. 9c), and temperature falls below $\lesssim 100 \text{ K}$. Thermal evolution finally converges to the HD-cooling track in the free-falling phase.

In our model for the shock-compressed gas, the contraction equations (eqs. 9, 10) are coupled with the energy equation (eq. 5) before the self gravity becomes effective, so that the timescale of the isobaric contraction phase differs among the lines. However, the evolution time after self-gravity becomes effective is almost the same and the time to reach $n = 10^5 \text{ cm}^{-3}$ is $\sim 50 \text{ Myr}$ for the structure-formation shock,

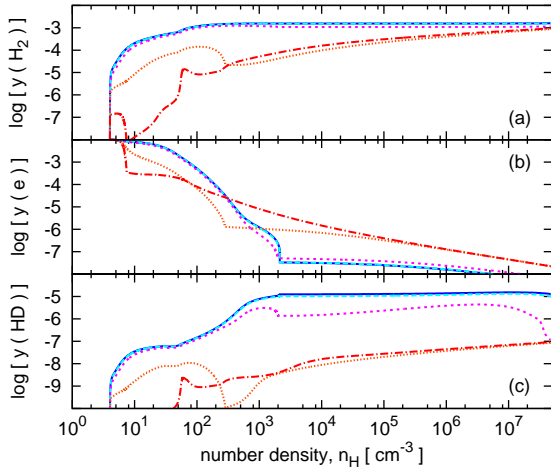


Figure 7. Fractions of (a) H_2 , (b) e , and (c) HD in the same clouds as in Fig. 6. Different lines correspond to the different FUV intensities: $J_{21} = 0.0$ (solid), 0.01 (long-dashed), 0.1 (short-dashed), 1.0 (dotted), and 10 (dot-dashed).

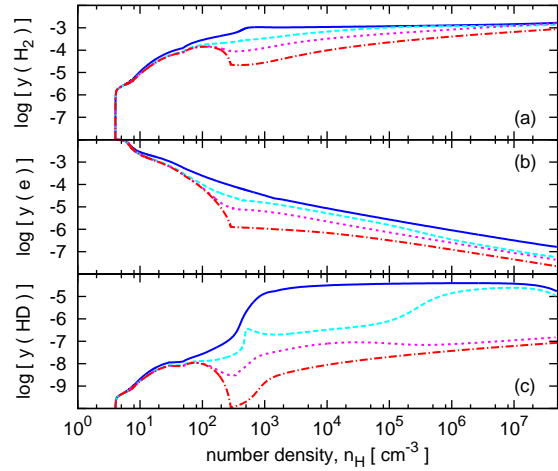


Figure 9. Fractions of (a) H_2 , (b) e , and (c) HD in the same clouds as in Fig. 8. The different lines correspond to the different CR intensities: $\log \zeta_{\text{CR}}(\text{s}^{-1}) = -\infty$ (dot-dashed), -19 (short-dashed), -18 (long-dashed), and -17 (solid).

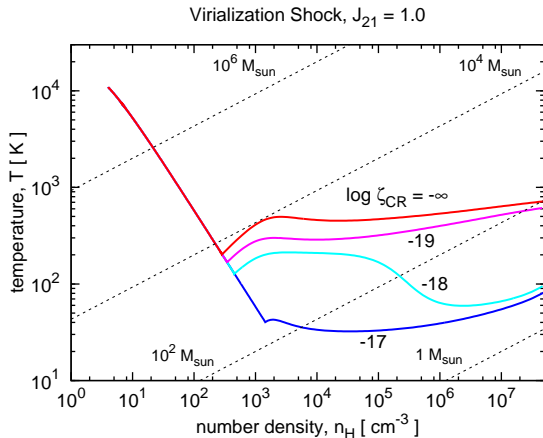


Figure 8. CR effect on the thermal evolution of shock-compressed clouds by virialization. The FUV intensity is fixed to $J_{21} = 1.0$. The initial density and velocity are the fiducial values: $n_{\text{H},0} = 1.0 \text{ cm}^{-3}$ and $v_0 = 20 \text{ km s}^{-1}$. The different lines correspond to the different CR intensities: $\log \zeta_{\text{CR}}(\text{s}^{-1}) = -\infty, -19, -18, \text{ and } -17$.

which is by an order of magnitude smaller than the local Hubble time $t_{\text{H}}(z) = 500 \left(\frac{1+z}{10} \right)^{-3/2} \text{ Myr}$ for $z < 15$. Thus, the shock-compressed gas in structure formation may be unaffected by the protogalaxy rotation and merger, and star formation there proceeds within the local Hubble time.

3.2.2 Supernova Shock

In Fig. 10, we show the FUV effect on the shock-compressed gas in an SN explosion ($v_0 = 100 \text{ km s}^{-1}$) for cases without CR irradiation. We find that, despite the different initial conditions, the evolutionary tracks are similar to those in the virialization shock with the same FUV intensity (see Fig. 6). This is because, although the initial density $n_{\text{H},0} = 0.1 \text{ cm}^{-3}$ is ten times lower in the SN case, the post-shock temperature is 25 times higher and thus the pressure in the isobaric evolution phase differs only by a factor of 2.5 (see Fig. 6). We also find that the chemical compositions vary in a similar way as in the case of virialization shock (see Fig. 7), except that the ionization degree reaches ~ 1 due to the very high temperature $\sim 10^5 \text{ K}$ behind the SN shock front.

The same trend holds also in the cases with CR irradiation, and the evolutionary tracks are similar to those in the virialization shock with the same CR intensity (see Figs. 8 and 11).

For the SN-shock case, the evolution time after self-gravity becomes effective is almost the same and the time to reach $n = 10^5 \text{ cm}^{-3}$ is calculated as $\sim 250 \text{ Myr}$, which is much longer than the lifetime of an SN remnant $\sim 1 \text{ Myr}$. Thus, the SN shock will dissolve into the ISM before it collects enough materials to trigger fragmentation and star formation in the post-shock region. This result is consistent with Chiaki et al. (2013), where they find that the SN-shock-compressed gas can collapse within the lifetime of the SN remnant for the ISM density $\gtrsim 1 \text{ cm}^{-3}$ and $E_{\text{SN}} = 10^{51} \text{ erg}$. However, we discuss the evolution of the SN-shock-compressed gas for comparison with that of structure formation.

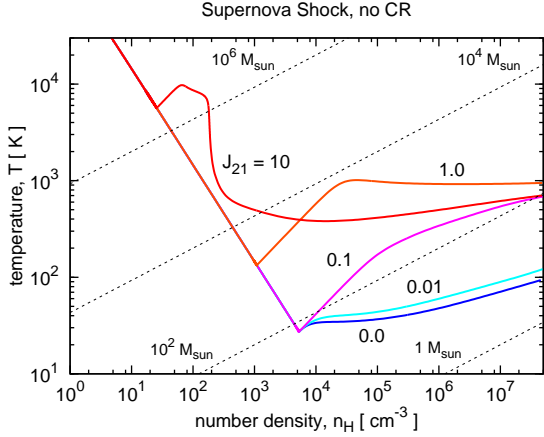


Figure 10. FUV effect on the thermal evolution of shock-compressed clouds by SNe. No CR irradiation is considered. The fiducial initial conditions are adopted: $n_{\text{H},0} = 0.1 \text{ cm}^{-3}$ and $v_0 = 100 \text{ km s}^{-1}$. The different lines correspond to the different FUV intensities: $J_{21} = 0.0, 0.01, 0.1, 1.0,$ and 10 .

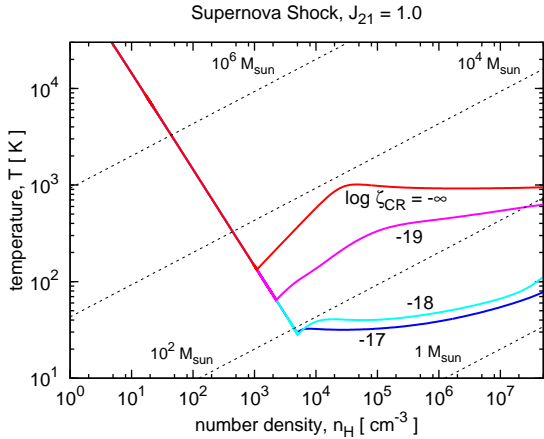


Figure 11. CR effect on the same clouds as in Fig. 10. The FUV intensity is fixed to $J_{21} = 1.0$. The different lines correspond to the different CR intensities: $\log \zeta_{\text{CR}} (\text{s}^{-1}) = -\infty, -19, -18,$ and -17 .

3.2.3 Critical FUV intensity for HD Cooling

As in §3.1.2, the critical FUV intensity for HD cooling $J_{21,\text{crit}}$ is calculated for a shock-compressed gas and is presented in Fig. 12 as a function of the CR intensity ζ_{CR} . The solid and dashed lines are for the virialization shock in the fiducial case $(v_0, n_{\text{H},0}) = (20, 1.0)$ and in the high density case $(v_0, n_{\text{H},0}) = (20, 10)$, respectively, and the dot-dashed line indicates the SN shock case $(v_0, n_{\text{H},0}) = (100, 0.1)$.

From Fig. 12, we see that for $\log \zeta_{\text{CR}} \lesssim -18$, the critical value $J_{21,\text{crit}}$ becomes higher for a higher initial density $n_{\text{H},0}$ or higher shock velocity v_0 . The reason is the same as in the case of a relic HII region: in the weak CR regime,

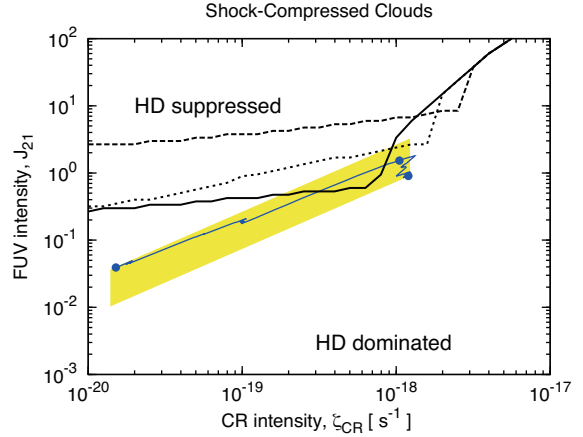


Figure 12. The critical FUV intensity $J_{21,\text{crit}}$ for HD cooling as a function of the CR intensity ζ_{CR} in shock-compressed clouds (see also Fig. 5). The solid and dashed lines correspond to the virialization shock with the fiducial case, $(v_0, n_{\text{H},0}) = (20, 1.0)$, and the high density case, $(v_0, n_{\text{H},0}) = (20, 10)$, respectively. The dot-dashed line shows the SN-shock case, $(v_0, n_{\text{H},0}) = (100, 0.1)$.

abundant H_2/HD formation is caused by the high post-shock ionization degree, and thus the prompt FUV shielding before significant recombination is needed. This can be realized more easily with a higher initial density $n_{\text{H},0}$ or higher shock velocity v_0 , since the column density at $\sim 10^4 \text{ K}$, below which recombination proceeds significantly, is higher in these cases. On the other hand, for $\log \zeta_{\text{CR}} \gtrsim -18$, the critical value $J_{21,\text{crit}}$ is solely determined by the CR strength ζ_{CR} and becomes independent of the initial condition $(n_{\text{H},0}, v_0)$. Again the reason is the same as in the relic-HII-region case: the electrons from CR ionization, rather than those present initially, now work as catalysts for H_2 formation and thus the H_2 formation rate does not depend on the initial parameters.

The comparison between Figs. 5 and 12 tells us that in the weak CR regime, $\log \zeta_{\text{CR}} \lesssim -19$, the critical intensity is ~ 10 times higher for the shock-compressed gas ($\log J_{21,\text{crit}} = -0.5 \dots 0.5$) than in the relic HII region ($\log J_{21,\text{crit}} = -2 \dots -1$). In this case, for abundant H_2/HD formation, H_2 should be promptly shielded against the FUV field before the electrons present initially recombine significantly. This condition can be more easily satisfied in the shock-compressed gas than in the relic HII region. The reason is that the shock-compressed gas evolves isobarically (see Fig. 6) rather than isochorically as in the relic HII region (see Fig. 1), which leads to the larger column density in the shock-compressed gas. In addition, shocks tend to occur in denser environments (e.g., cold-accretion flows) than relic HII regions. Consequently, in the shock-compressed gas, H_2 is shielded from the FUV field more effectively, and the critical FUV intensity becomes higher than that in the relic HII region.

4 ESTIMATE FOR BACKGROUND INTENSITIES

We have seen that Pop III.2 star formation proceeds through the HD-cooling track, i.e., in the HD-Pop III star formation mode, under a weak FUV field or strong enough CR irradiation. In this section, we estimate the intensities of the FUV and CR backgrounds as a function of redshift. Then, by comparing them with the critical value $J_{21,\text{crit}}$ obtained in §3, we discuss whether HD-Pop III star formation is realized at the epoch of galaxy formation ($z \lesssim 15$).

At this epoch, metal enrichment in an average galaxy may have proceeded to the level for Pop II star formation to occur (e.g., Wise et al. 2012; Johnson et al. 2013). We thus consider massive Pop II stars and their SN remnants as the plausible sources of the FUV and CR backgrounds, respectively. Then, the intensity of the FUV background is estimated as (Greif & Bromm 2006)

$$J_{\text{LW,bg}}(z) = \frac{hc}{4\pi m_{\text{H}}} \frac{\bar{\nu}}{\Delta\nu} \eta_{\text{LW}} \rho_*(z) (1+z)^3, \quad (17)$$

where h is the Planck constant, c the speed of light, $\bar{\nu}$ the average frequency of the LW band ($h\bar{\nu} = 12.4$ eV), $\Delta\nu$ the LW band width ($h\Delta\nu = 2.4$ eV), $\eta_{\text{LW}} = 4000$ the number of FUV photons emitted per stellar baryon, and $\rho_*(z)$ the stellar mass density at z . Johnson et al. (2013) evaluated $\rho_*(z)$ by the relation $\rho_*(z) = \Psi_{*,\text{II}}(z) t_*$, where $\Psi_{*,\text{II}}(z)$ is the Pop II SFR density, and $t_* = 5$ Myr the lifetime of a massive star. Then, Eq. (17) can be rewritten as

$$J_{21,\text{bg}}(z) \sim 0.1 \left(\frac{\Psi_{*,\text{II}}(z)}{10^{-3} \text{ M}_{\odot} \text{ yr}^{-1} \text{ Mpc}^{-3}} \right) \left(\frac{1+z}{11} \right)^3. \quad (18)$$

Following Stacy & Bromm (2007), the energy density of the background CRs $U_{\text{CR}}(z)$ is estimated from

$$U_{\text{CR}}(z) \sim p_{\text{CR}} E_{\text{SN}} f_{\text{SN}} \Psi_{*,\text{II}}(z) t_{\text{H}}(z) (1+z)^3, \quad (19)$$

$$\sim 4 \times 10^{-17} \left(\frac{\Psi_{*,\text{II}}(z)}{10^{-3} \text{ M}_{\odot} \text{ yr}^{-1} \text{ Mpc}^{-3}} \right) \left(\frac{1+z}{11} \right)^{\frac{3}{2}} \text{ erg cm}^{-3},$$

where $E_{\text{SN}} = 10^{51}$ erg is the SN energy, $p_{\text{CR}} = 0.1$ the efficiency of E_{SN} converted to CR acceleration, f_{SN} the number of SNe per unit mass of stars formed, and $t_{\text{H}}(z)$ the Hubble time at z . f_{SN} is obtained as $\sim 2 \times 10^{-2} \text{ M}_{\odot}^{-1}$ assuming that massive stars with $\gtrsim 8 \text{ M}_{\odot}$ explode as SNe for the Salpeter IMF. The CR ionization rate of a hydrogen atom ζ_{CR} is related with U_{CR} as (Inayoshi & Omukai 2011):

$$\zeta_{\text{CR}} = 1.7 \times 10^{-18} \left(\frac{U_{\text{CR}}}{10^{-15} \text{ erg cm}^{-3}} \right) \text{ s}^{-1}. \quad (20)$$

Combining Eqs. (19) and (20),

$$\zeta_{\text{CR}}(z) \sim 6.8 \times 10^{-20} \left(\frac{\Psi_{*,\text{II}}(z)}{10^{-3} \text{ M}_{\odot} \text{ yr}^{-1} \text{ Mpc}^{-3}} \right) \left(\frac{1+z}{11} \right)^{\frac{3}{2}} \text{ s}^{-1}. \quad (21)$$

The high- z SFR density has been evaluated theoretically by some authors (e.g., Tornatore et al. 2007; Trenti & Stiavelli 2009; Johnson et al. 2013). According to Johnson

et al. (2013), $\Psi_{*,\text{II}}(z)$ increases almost monotonically from 10^{-4} to $3 \times 10^{-2} \text{ M}_{\odot} \text{ yr}^{-1} \text{ Mpc}^{-3}$ as z decreases from 15 to 6. The blue thin-solid lines in Figs. 5 and 12 show the evolution of $J_{21,\text{bg}}(z)$ and $\zeta_{\text{CR}}(z)$ evaluated from Eqs. (18), (21) and $\Psi_{*,\text{II}}(z)$ of Johnson et al. (2013). The background intensities move from left to right along the line, and the blue points indicate the values at $z = 15, 10$ and 6 , respectively. Although the high- z SFR density is still uncertain, most studies concluded $10^{-4} \lesssim \Psi_{*,\text{II}}(z) / \text{M}_{\odot} \text{ yr}^{-1} \text{ Mpc}^{-3} \lesssim 3 \times 10^{-2}$ for $6 \lesssim z \lesssim 15$ (e.g., Tornatore et al. 2007; Trenti & Stiavelli 2009; Johnson et al. 2013). The shaded regions in Figs. 5 and 12 indicate the range of $J_{21,\text{bg}}(z)$ and $\zeta_{\text{CR}}(z)$ corresponding to this parameter range.

First, we examine the case of free-falling clouds in relic HII regions (Fig. 5). For initial densities lower than the fiducial case $n_{\text{H},0} = 0.3 \text{ cm}^{-3}$ (black solid line), the critical FUV intensity for HD cooling $J_{21,\text{crit}}$ is below the background level $J_{21,\text{bg}}$ at $z \gtrsim 10$, and HD cooling is suppressed in Pop III.2 star formation. As the background CR intensity ζ_{CR} increases with cosmic star formation, the critical intensity $J_{21,\text{crit}}$ rises and eventually exceeds the background level $J_{21,\text{bg}}$ at $z \lesssim 10$. Below this redshift, HD cooling becomes efficient and HD-Pop III star formation occurs if some primordial environments still survive. Although in a very dense HII region (dot-dashed line), the critical intensity $J_{21,\text{crit}}$ is above the background level $J_{21,\text{bg}}$ even at $z \gtrsim 10$, such dense conditions appear to be hardly realized (Kitayama et al. 2004; Whalen et al. 2004; Yoshida et al. 2007a, Abel 2007). We conclude that, in relic HII regions, HD-Pop III star formation is possible only at $z \lesssim 10$, where the intensity of the CR background is modest.

On the other hand, for the shock-compressed gas (Fig. 12), the critical value $J_{21,\text{crit}}$ exceeds the background level $J_{21,\text{bg}}$ for most of the redshift we consider ($6 \lesssim z \lesssim 15$), and thus HD-Pop III star formation occurs. Note that the pre-shock densities we adopt in Fig. 12 are rather low, and our results may give the lower bound of the critical FUV intensity $J_{21,\text{crit}}$. In fact, in the mass assembly process of first galaxies, cold-streaming shocks occur at the regions as dense as $n_{\text{H},0} = 1\text{--}10^3 \text{ cm}^{-3}$ (Wise & Abel 2007; Wise et al. 2008). In such a dense shock environment, HD-Pop III star formation would be more common than the cases we have studied. In conclusion, the HD-Pop III mode is the main mode of Pop III.2 star formation in the cloud compressed either by a virialization or SN shock.

5 DISCUSSION

So far, we have considered that the background FUV photons are uniformly distributed in the universe. In reality, they have some spatial fluctuations caused by local stellar sources, like star-forming galaxies (Dijkstra et al. 2008; Ahn et al. 2009; Agarwal et al. 2012; Johnson et al. 2013). In the primordial clouds irradiated with the strong FUV field as $J_{21} > 3$, HD formation is suppressed even in the shock-compressed gas unless the initial density is high (10 cm^{-3}) or the CR intensity is strong ($> 10^{-18} \text{ s}^{-1}$; see Fig. 12). However, according to Johnson et al. (2013), only $\lesssim 10$ percent of

the dense primordial cloud with $n_{\text{H}} > 1 \text{ cm}^{-3}$ is exposed to such a strong FUV field as $J_{21} > 3$. Thus, our analysis with the uniform background FUV field is enough to discuss the major character of primordial star formation and the spatial fluctuations of it do not affect our main conclusions.

We also assume that CRs accelerated in SN remnants escape freely from their host galaxies and fill the universe homogeneously. However, in reality, they may be trapped in the host galaxy by the interaction with the magnetic field, and propagate diffusively through the ISM of the galaxy (Longair 2011). On the way of propagation, CRs also lose their kinetic energy by ionizing the neutral ISM. For the efficient CR escape into the IGM, the CR escape time by diffusion τ_{diff} should be shorter than both the ionization loss time τ_{ion} and the age of the system τ_{age} , which is roughly equal to the age of the universe. Here, τ_{diff} and τ_{ion} depends on the kinetic energy of a CR particle E and the redshift z . Rollinde et al. (2008) estimated the above timescales for CRs with $E = 30 \text{ MeV}$ and discussed the CR escape efficiency during the cosmic structure formation. Here, we extend their arguments by examining the E dependence of the timescales. Following Stacy & Bromm (2007), we assume that the energy spectrum of the CR number density has a power-law shape $dn_{\text{CR}}/dE \propto E^{-x}$ with $E = 10^6\text{-}10^{15} \text{ eV}$. We find that the inequality $\tau_{\text{diff}}(E, z) < \tau_{\text{age}}(z)$ holds for all the CR energy and redshift we consider ($6 \lesssim z \lesssim 15$). On the other hand, the inequality $\tau_{\text{diff}}(E, z) < \tau_{\text{ion}}(E, z)$ holds only for high energy CRs with $E \gtrsim 10^7 \text{ eV}$ at $6 \lesssim z \lesssim 15$. Thus, the CR background is composed of CRs with $E \gtrsim 10^7 \text{ eV}$ and its intensity varies with the spectrum index x . In the standard Fermi acceleration theory, the spectrum index is given as $x = 2$ (e.g., Bell 1978), and the background intensity is reduced only by 10 % due to the confinement of CRs with $E = 10^6\text{-}10^7 \text{ eV}$. On the other hand, if we adopt a steeper slope as $x = 3$ in Rollinde et al. (2008), it is reduced by an order of magnitude. Even in this case, if a star-forming pristine gas resides in the same galaxy hosting SNe, it is exposed to the CR intensity in the original or even the enhanced level, because of the efficient confinement within the galaxy. For more quantitative and definitive discussions, a detailed study of CR propagation in the ISM of high- z galaxies is needed and is beyond the scope of this paper.

At the epoch of galaxy formation, high-mass X-ray binaries and miniquasars may be the plausible sources of high energy photons extending to the X-ray band (Glover & Brand 2003). Since the photoionization cross section of neutral atoms generally decreases with frequency in the power-law way, the IGM becomes optically thin for X-ray photons with $\gtrsim 1 \text{ keV}$ and the X-ray background develops at this epoch (Haiman et al. 2000). The injection of X-ray photons enhances the cooling efficiency of primordial clouds by indirectly promoting H_2 and HD formation through the photoionization of neutral atoms (e.g., Haiman, Rees & Loeb 1996; Haiman, Abel & Rees 2000; Glover & Brand 2003; Machacek, Bryan & Abel 2003). Nonetheless, we did not include this X-ray feedback, and here we briefly discuss how it changes our results. Following Glover & Brand (2003), we assume that the X-ray background has a power-law spec-

trum

$$J_{\text{X}}(\nu) = J_{\text{X},21} \times 10^{-21} \left(\frac{\nu}{1 \text{ keV}} \right)^{-1.5} \text{ erg cm}^{-2} \text{ s}^{-1} \text{ Hz}^{-1}, \quad (22)$$

where $J_{\text{X},21} \equiv J_{1\text{keV}}/10^{-21} \text{ erg cm}^{-2} \text{ s}^{-1} \text{ Hz}^{-1}$ and $J_{1\text{keV}}$ is the intensity at 1 keV. Then, using Eqs. (17-19) in Inayoshi & Omukai (2011), the ionization rate of H is calculated as

$$\zeta_{\text{X}}^{\text{H}} \sim 2 \times 10^{-15} J_{\text{X},21} \text{ s}^{-1}, \quad (23)$$

for the hydrogen column density $N_{\text{H}} \lesssim 10^{22} \text{ cm}^{-2}$. Since the background field derives from the stellar activity, the X-ray intensity is related with the CR energy density as

$$J_{\text{X},21} \sim 10^{-3} \left(\frac{U_{\text{CR}}}{10^{-15} \text{ erg cm}^{-3}} \right), \quad (24)$$

where we suppose that CR sources are Pop II clusters with the Salpeter IMF and the mass range 1-100 M_{\odot} (Inayoshi & Omukai 2011)³. Substituting Eq. (20) into Eq. (24) and Eq. (24) into Eq. (23), the X-ray ionization rate is related with the CR ionization rate as

$$\zeta_{\text{X}}^{\text{H}} \sim \zeta_{\text{CR}}. \quad (25)$$

Thus, we find that, at each redshift, X-ray feedback changes the ionization rate in pristine clouds not by an order of magnitude, but by only up to a factor of two. Note that this is the upper limit of the X-ray effect since X-ray is more effectively shielded than CRs. Therefore, our main conclusion still remains valid even if we consider X-ray feedback.

As we have seen above, Pop III star formation at the epoch of galaxy formation is affected significantly by the injection of CRs. Nonetheless, some previous studies calculated the Pop III SFR by considering the regulation process of star formation from FUV feedback alone, and the positive feedback from CRs is neglected (e.g., Tornatore et al. 2007; Trenti & Stiavelli 2009; de Souza et al. 2011; Johnson et al. 2013). Future studies should take all these feedback into consideration.

We must admit that our treatment of the plane-parallel and steady shock is too simplistic to capture possible complex phenomena induced by e.g., the turbulence, rotation, thermal instability, and magnetic field. For example, Inoue & Inutsuka (2008, 2009) studied the effect of magnetic fields on the thermal evolution of a shock-compressed gas, using the two-dimensional MHD simulation. They found that after the short isobaric contraction, the magnetic pressure is amplified to be comparable to the ram pressure of the pre-shock materials, and thereafter the shock-compressed gas cools almost isochorically. This implies that the shielding of H_2 against a FUV field becomes less effective and the resultant H_2 fraction is lowered in the presence of magnetic fields. In this case, we expect that more massive clumps may form after the gas becomes gravitationally

³ We adopt $E_{\text{SN}} = 10^{51} \text{ erg}$ as the energy of a Pop II SN instead of $E_{\text{SN}} = 10^{52} \text{ erg}$ in Inayoshi & Omukai (2011).

unstable and fragments, compared to the isobaric contraction case without magnetic fields. However, their calculation did not follow the evolution until the self-gravity of the shocked layer becomes important. They did not consider the gas in the primordial composition as well. Thus, the above effects on our results should be investigated through the 3D MHD simulations in the future. Another example is that our assumption of the time-independent shock velocity becomes invalid at least in the SN-shock, according to the one-dimensional numerical calculations (Machida et al. 2005; Nagakura, Hosokawa & Omukai 2009; Chiaki, Yoshida & Kitayama 2013). They showed that the SN-shock velocity becomes lower than 100 km s^{-1} at $\sim 10^5 \text{ yr}$ after the explosion. Moreover, at $\gtrsim 6 \times 10^5 \text{ yr}$, the ram pressure of the ambient medium decreases below the pressure in the shell so that the shell re-expands and decreases its temperature and density in an almost adiabatic manner. Although in this case, H_2 is produced efficiently to $\sim 10^{-3}$ and the temperature decreases to $\sim 200 \text{ K}$ by H_2 cooling, HD is produced only to $\sim 10^{-6}$, which is ~ 10 times less than our results, in the adiabatic expansion phase owing to the low gas density. In this case, the temperature decrease below 100 K is not caused by HD cooling but by the adiabatic expansion of the shell (Nagakura, Hosokawa & Omukai 2009). However, if the SN shock can collect enough materials to trigger gas fragmentation and contraction by self-gravity before dissolving into the ISM, HD formation becomes effective and HD cooling becomes dominated in the free-falling phase, as we can see from Fig. 6 in Machida et al. (2005) and Fig. 6 in Chiaki, Yoshida & Kitayama (2013). Thus, whether this realistic evolution of the SN shock front significantly changes our results is not clear, and more detailed numerical calculations are needed for more concrete discussion.

6 CONCLUSIONS

HD molecules form abundantly in the primordial gas with enhanced initial ionization and play a dominant role in gas cooling. At the epoch of galaxy formation ($z \lesssim 15$), shocks occur ubiquitously associated with the mass assembly as well as the SN explosions. In such a shock-compressed gas, the ionization degree jumps up owing to collisional ionization. Other examples include the cloud in the relic HII region of a defunct Pop III star and that with modest CR irradiation. However, even a low level of the FUV background suppresses HD formation/cooling via H_2 photodissociation in cases without CR irradiation. In this paper, we have examined the conditions for efficient HD cooling in primordial star formation by calculating the thermal and chemical evolution of a gas cloud under both FUV and CR irradiation. We have obtained the critical FUV intensity $J_{21,\text{crit}}$ for HD cooling as a function of the CR intensity ζ_{CR} , and compared it with the estimated background level $J_{21,\text{bg}}$. We have considered both cases of the free-falling cloud in a relic HII region and a shock-compressed gas.

At $z \gtrsim 10$, the background CR intensity is estimated as $\sim 0.1 \%$ of the Galactic value. In this case, the critical FUV intensity $J_{21,\text{crit}}$ in relic HII regions is below the background

level $J_{21,\text{bg}}$ and HD cooling is suppressed there. However, as the background CR intensity increases with the cosmic star formation, the critical intensity $J_{21,\text{crit}}$ is also elevated and eventually exceeds the background level $J_{21,\text{bg}}$ at $z \lesssim 10$. Below this redshift, HD cooling becomes efficient and HD-Pop III star formation proceeds if some primordial environments still survive.

On the other hand, the critical FUV intensity $J_{21,\text{crit}}$ for the shock-compressed gas is ~ 10 times higher than that for the relic HII region even in the weak CR regime as $\sim 0.1 \%$ of the Galactic value. This is because the shock-compressed gas evolves isobarically (i.e., gas cools with its density increasing), while the gas in a relic HII region evolves isochorically (i.e., the gas cools at a constant density) due to the initial rapid cooling. Moreover, shocks tend to occur in denser environments (e.g., cold-accretion flows) than relic HII regions. As a result, the shock-compressed gas is shielded from the FUV field more effectively, and has higher critical intensity. Thus, for the shock-compressed gas, the critical value $J_{21,\text{crit}}$ exceeds the background level $J_{21,\text{bg}}$ and HD-Pop III star formation proceeds for most of the redshift we consider ($6 \lesssim z \lesssim 15$).

Our result suggests that HD-Pop III stars can be more common than previously considered and could be even the dominant population of Pop III stars. H_2 -Pop III stars are born in clumps as massive as $\sim 10^3 M_\odot$, but the final stellar mass is set to $\sim 100 M_\odot$ by the stellar radiative feedback onto the accretion flow (McKee & Tan 2008; Hosokawa et al. 2011; Hirano et al. 2014). On the other hand, HD-Pop III stars form in clumps of $\sim 100 M_\odot$, and the final mass is typically set to a few $10 M_\odot$ by the stellar feedback (Hosokawa et al. 2012). These previous results may suggest that the star formation efficiency, i.e., the mass ratio of formed stars to the parent clouds, of HD-Pop III stars is several times higher than that of H_2 -Pop III stars. They also imply the possibility that HD-Pop III stars could be the majority of Pop III.2 stars. Then, HD-Pop III stars of a few $10 M_\odot$ can be important sources of radiative feedback at the epoch of galaxy formation. Moreover, according to the observations of the abundance patterns in the metal-poor halo stars in the Galaxy, the imprints of a pair-instability SN have not been discovered yet (Tumlinson, Venkatesan & Shull 2004; Frebel, Johnson & Bromm 2009). Since stars with $10\text{-}40 M_\odot$ end their lives as core-collapse SNe (Heger et al. 2003), HD-Pop III stars might be the major contributor to the metal enrichment in the ISM/IGM at that epoch, if there were no PISNe in the universe.

Recent discoveries of the almost pristine gas with metallicity $\lesssim 10^{-4} Z_\odot$ in the damped Ly α systems at $z \sim 3$ and 7 (Fumagalli, O’Meara & Prochaska 2011; Simcoe et al. 2012) imply that metal enrichment in the IGM has proceeded quite inhomogeneously. Theoretical models also show the inhomogeneous nature of metal enrichment in the IGM. They predict that Pop III star formation can continue up to $z \sim 6$ or even lower, and evaluate the ratio of the Pop III SFR to the total SFR as $\sim 10^{-3}\text{-}10^{-2}$ ($\sim 10^{-4}$) at $z = 10$ ($z = 6$) (Tornatore et al. 2007; Johnson et al. 2013). This indicates that Pop III stars can form to some extent even at $z \lesssim 10$, and our study show that they are typically

formed as HD-Pop III stars with a few $10 M_{\odot}$. GRBs and SNe from these Pop III progenitors at $z \lesssim 10$ will be detected with the current or future facilities and may provide us with information on the mass, IMF and SFR of these stars (Nakauchi et al. 2012; Whalen et al. 2013; Tanaka et al. 2013). Moreover, if the HD absorption lines are detected in the spectrum of a GRB afterglow which lacks metal absorption, HD is confirmed as the dominant coolant in that primordial gas (Inoue, Omukai & Ciardi 2007).

ACKNOWLEDGEMENTS

We thank the anonymous referee for helpful comments and improving the quality of this paper. We also thank K. Kashiyama, T. Nakamura, Y. Suwa, and K. Tanaka for fruitful discussions and comments. This work is supported in part by the Grant-in-Aid from the Ministry of Education, Culture, Sports, Science and Technology (MEXT) of Japan (23-838 KI; 25287040 KO).

REFERENCES

- Abel, T., Bryan, G. L., & Norman, M. L. 2002, *Science*, 295, 93
- Abel, T., Wise, J. H., & Bryan, G. L. 2007, *ApJ*, 659, L87
- Agarwal, B., Khochfar, S., Johnson, J. L., et al. 2012, *MNRAS*, 425, 2854
- Ahn, K., Shapiro, P. R., Iliiev, I. T., Mellema, G., & Pen, U.-L. 2009, *ApJ*, 695, 1430
- Bell, A. R. 1978, *MNRAS*, 182, 147
- Bromm, V., Coppi, P. S., & Larson, R. B. 1999, *ApJ*, 527, L5
- Bromm, V., Coppi, P. S., & Larson, R. B. 2002, *ApJ*, 564, 23
- Bromm, V., Yoshida, N., & Hernquist, L. 2003, *ApJ*, 596, L135
- Chiaki, G., Yoshida, N., & Kitayama, T. 2013, *ApJ*, 762, 50
- Ciardi, B., & Ferrara, A. 2005, *Space Sci. Rev.*, 116, 625
- Clarke, C. J., & Bromm, V. 2003, *MNRAS*, 343, 1224
- Couchman, H. M. P., & Rees, M. J. 1986, *MNRAS*, 221, 53
- de Souza, R. S., Yoshida, N., & Ioka, K. 2011, *A&A*, 533, A32
- Dijkstra, M., Haiman, Z., Mesinger, A., & Wyithe, J. S. B. 2008, *MNRAS*, 391, 1961
- Frebel, A., Johnson, J. L., & Bromm, V. 2009, *MNRAS*, 392, L50
- Fumagalli, M., O’Meara, J. M., & Prochaska, J. X. 2011, *Science*, 334, 1245
- Galli, D., & Palla, F. 1998, *A&A*, 335, 403
- Galli, D., & Palla, F. 2002, *Planet. Space Sci.*, 50, 1197
- Glover, S. C. O., & Abel, T. 2008, *MNRAS*, 388, 1627
- Glover, S. C. O., & Brand, P. W. J. L. 2001, *MNRAS*, 321, 385
- Glover, S. C. O., & Brand, P. W. J. L. 2003, *MNRAS*, 340, 210
- Glover, S. C. O., & Jappsen, A.-K. 2007, *ApJ*, 666, 1
- Greif, T. H., & Bromm, V. 2006, *MNRAS*, 373, 128
- Greif, T. H., Johnson, J. L., Klessen, R. S., & Bromm, V. 2008, *MNRAS*, 387, 1021
- Greif, T. H., Bromm, V., Clark, P. C., et al. 2012, *MNRAS*, 424, 399
- Haiman, Z., Rees, M. J., & Loeb, A. 1996, *ApJ*, 467, 522
- Haiman, Z., Thoul, A. A., & Loeb, A. 1996, *ApJ*, 464, 523
- Haiman, Z., Rees, M. J., & Loeb, A. 1997, *ApJ*, 476, 458
- Haiman, Z., Abel, T., & Rees, M. J. 2000, *ApJ*, 534, 11
- Hayakawa, S., Nishimura, S., & Takayanagi, T. 1961, *PASJ*, 13, 184
- Heger, A., Fryer, C. L., Woosley, S. E., Langer, N., & Hartmann, D. H. 2003, *ApJ*, 591, 288
- Hirano, S., Hosokawa, T., Yoshida, N., et al. 2014, *ApJ*, 781, 60
- Hirasawa, T., Aizu, K., & Taketani, M. 1969, *Progress of Theoretical Physics*, 41, 835
- Hosokawa, T., Omukai, K., Yoshida, N., & Yorke, H. W. 2011, *Science*, 334, 1250
- Hosokawa, T., Yoshida, N., Omukai, K., & Yorke, H. W. 2012, *ApJ*, 760, L37
- Inayoshi, K., & Omukai, K. 2011, *MNRAS*, 416, 2748
- Inayoshi, K., & Omukai, K. 2012, *MNRAS*, 422, 2539
- Indriolo, N., Geballe, T. R., Oka, T., & McCall, B. J. 2007, *ApJ*, 671, 1736
- Inoue, S., Omukai, K., & Ciardi, B. 2007, *MNRAS*, 380, 1715
- Inoue, T., & Inutsuka, S.-i. 2008, *ApJ*, 687, 303
- Inoue, T., & Inutsuka, S.-i. 2009, *ApJ*, 704, 161
- Jasche, J., Ciardi, B., & Enßlin, T. A. 2007, *MNRAS*, 380, 417
- Johnson, J. L., & Bromm, V. 2006, *MNRAS*, 366, 247
- Johnson, J. L., Dalla, Vecchia, C., & Khochfar, S. 2013, *MNRAS*, 428, 1857
- Kang, H., & Shapiro, P. R. 1992, *ApJ*, 386, 432
- Kitayama, T., Yoshida, N., Susa, H., & Umemura, M. 2004, *ApJ*, 613, 631
- Larson, R. B. 1969, *MNRAS*, 145, 271
- Longair, M. S. 2011, *High Energy Astrophysics*, by Malcolm S. Longair, Cambridge, UK: Cambridge University Press, 2011
- Machacek, M. E., Bryan, G. L., & Abel, T. 2003, *MNRAS*, 338, 273
- Machida, M. N., Tomisaka, K., Nakamura, F., & Fujimoto, M. Y. 2005, *ApJ*, 622, 39
- Mackey, J., Bromm, V., & Hernquist, L. 2003, *ApJ*, 586, 1
- McCall, B. J., Huneycutt, A. J., Saykally, R. J., et al. 2003, *Nature*, 422, 500
- McGreer, I. D., & Bryan, G. L. 2008, *ApJ*, 685, 8
- McKee, C. F., & Tan, J. C. 2008, *ApJ*, 681, 771
- Nagakura, T., & Omukai, K. 2005, *MNRAS*, 364, 1378
- Nagakura, T., Hosokawa, T., & Omukai, K. 2009, *MNRAS*, 399, 2183
- Nakamura, F., & Umemura, M. 2002, *ApJ*, 569, 549
- Nakauchi, D., Suwa, Y., Sakamoto, T., Kashiyama, K., & Nakamura, T. 2012, *ApJ*, 759, 128
- Omukai, K., & Nishi, R. 1999, *ApJ*, 518, 64
- Omukai, K. 2001, *ApJ*, 546, 635

- Omukai, K., & Palla, F. 2001, *ApJ*, 561, L55
Omukai, K., & Palla, F. 2003, *ApJ*, 589, 677
Omukai, K., Tsuribe, T., Schneider, R., & Ferrara, A. 2005, *ApJ*, 626, 627
Omukai, K. 2007, *PASJ*, 59, 589
O'Shea, B. W., Abel, T., Whalen, D., & Norman, M. L. 2005, *ApJL*, 628, L5
O'Shea, B. W., McKee, C. F., Heger, A., & Abel, T. 2008, *First Stars III*, 990, 13
O'Shea, B. W., & Norman, M. L. 2008, *ApJ*, 673, 14
Peebles, P. J. E., & Dicke, R. H. 1968, *ApJ*, 154, 891
Penston, M. V. 1969, *MNRAS*, 144, 425
Ritter, J. S., Safranek-Shrader, C., Gnat, O., Milosavljević, M., & Bromm, V. 2012, *ApJ*, 761, 56
Rollinde, E., Maurin, D., Vangioni, E., Olive, K. A., & Inoue, S. 2008, *ApJ*, 673, 676
Safranek-Shrader, C., Bromm, V., & Milosavljević, M. 2010, *ApJ*, 723, 1568
Schaerer, D. 2002, *A&A*, 382, 28
Shapiro, P. R., & Kang, H. 1987, *ApJ*, 318, 32
Simcoe, R. A., Sullivan, P. W., Cooksey, K. L., et al. 2012, *Nature*, 492, 79
Spitzer, L., Jr., & Tomasko, M. G. 1968, *ApJ*, 152, 971
Spitzer, L., Jr., & Scott, E. H. 1969, *ApJ*, 158, 161
Stacy, A., & Bromm, V. 2007, *MNRAS*, 382, 229
Stacy, A., Greif, T. H., & Bromm, V. 2012, *MNRAS*, 42
Susa, H. 2013, *ApJ*, 773, 185
Tanaka, M., Moriya, T. J., & Yoshida, N. 2013, *MNRAS*, 435, 2483
Tegmark, M., Silk, J., Rees, M. J., et al. 1997, *ApJ*, 474, 1
Tornatore, L., Ferrara, A., & Schneider, R. 2007, *MNRAS*, 382, 945
Trenti, M., & Stiavelli, M. 2009, *ApJ*, 694, 879
Tumlinson, J., Venkatesan, A., & Shull, J. M. 2004, *ApJ*, 612, 602
Uehara, H., & Inutsuka, S. I. 2000, *ApJL*, 531, L91
Wada, K., & Venkatesan, A. 2003, *ApJ*, 591, 38
Webber, W. R. 1998, *ApJ*, 506, 329
Whalen, D., Abel, T., & Norman, M. L. 2004, *ApJ*, 610, 14
Whalen, D. J., Fryer, C. L., Holz, D. E., et al. 2013, *ApJL*, 762, L6
Wise, J. H., & Abel, T. 2007, *ApJ*, 665, 899
Wise, J. H., Turk, M. J., & Abel, T. 2008, *ApJ*, 682, 745
Wise, J. H., Turk, M. J., Norman, M. L., & Abel, T. 2012, *ApJ*, 745, 50
Wolcott-Green, J., & Haiman, Z. 2011, *MNRAS*, 412, 2603
Yamada, M., & Nishi, R. 1998, *ApJ*, 505, 148
Yoshida, N., Omukai, K., Hernquist, L., & Abel, T. 2006, *ApJ*, 652, 6
Yoshida, N., Oh, S. P., Kitayama, T., & Hernquist, L. 2007, *ApJ*, 663, 687
Yoshida, N., Omukai, K., & Hernquist, L. 2007, *ApJ*, 667, L117
Yoshida, N., Omukai, K., & Hernquist, L. 2008, *Science*, 321, 669